Theor Chem Acc (2012) 131:1295
DOI 10.1007/s00214-012-1295-7

REGULAR ARTICLE

Singlet oxygen generation versus O–O homolysis in phenyl-substituted anthracene endoperoxides investigated by RASPT2, CASPT2, CC2, and TD-DFT methods

Stephan Kupfer · Guillermo Pérez-Hernández · Leticia González

Received: 28 August 2012 / Accepted: 20 October 2012

Abstract The electronic excited states corresponding to singlet oxygen generation versus O–O splitting in *o*-fluorine-phenyl-9-anthracene-9,10-endoperoxide **1** and its 9,10-bisarylanthracene analog **2** have been investigated using theoretical methods. In the case of the smaller endoperoxide **1**, the recently developed second-order perturbation theory restricted active space (RASPT2) method has been employed and the results are compared to those from the complete active space (CASPT2), second-order approximated coupled cluster (CC2), and time-dependent density functional theory (TD-DFT) approaches. In addition to the vertical excited states, the photochemical path leading to homolytic O–O dissociation has been computed. This process is governed by a point, where four singlet and four triplet states are almost degenerate and show substantial spin-orbit coupling. The results obtained with RASPT2 indicate that the S_1 state is of $\pi^*_{oo}\sigma^*_{oo}$ character, corresponding to the O–O homolytic dissociation, while higher excited states S_n ($n \geq 2$) correspond to local and charge transfer excitations and should be correlated to the generation of singlet molecular oxygen. A similar photochemical picture is obtained with CASPT2, although two different active spaces are required to describe different parts of the spectrum. The calculations carried out with CC2 as well as the functionals CAM-B3LYP and the B3LYP(32) containing 32 % of exact exchange show good agreement with the RASPT2 energies, but present a strong mixing of $\pi^*_{oo}\sigma^*_{oo}$ and $\pi^*_{oo}\ \pi^*_{an}$ excitations in the lowest S_1 state, contradicting the assignment of RASPT2/CASPT2. The use of BP86 is strongly discouraged since it misplaces a large number of charge transfer states below the $\pi^*_{oo}\sigma^*_{oo}$ state. The excited states of **2**, calculated with B3LYP(32) are very similar to those of **1**, leading to the conclusion that both endoperoxides should show a similar photochemistry, that is, the O–O cleavage seems to be partially quenched and singlet oxygen generation is enhanced, in comparison with the parent compound, anthracene-9,10-endoperoxide.

Keywords Ab initio calculations · DFT · Endoperoxides · Multiconfigurational methods · Singlet oxygen

1 Introduction

Endoperoxides of either aromatic or unsaturated organic compounds are well known for their capability of reversible oxygen storage [1, 2]. They can undergo a wide variety of reactions to form epoxides, carbonyl compounds or diols, among others. The capability of releasing the highly reactive singlet molecular oxygen ($^1O_2$) and other reactive oxygen species (ROS) makes endoperoxides attractive candidates in many fields of chemistry. In particular, the ROS play a key role in biological and biochemical processes [3]. Thanks to their great oxidation potential, ROS are key to photodynamic therapy [4], where their immense

Electronic supplementary material The online version of this article (doi:10.1007/s00214-012-1295-7) contains supplementary material, which is available to authorized users.

S. Kupfer · G. Pérez-Hernández
Institut für Physikalische Chemie, Friedrich-Schiller Universität Jena, Helmholzweg 4, 07743 Jena, Germany

Present Address:
G. Pérez-Hernández
Institut für Mathematik, Freie Universität Berlin, Arnimallee 6, 14195 Berlin, Germany

L. González (✉)
Institute of Theoretical Chemistry, University of Vienna, Währinger Strasse 17, 1090 Vienna, Austria
e-mail: leticia.gonzalez@univie.ac.at

Published online: 13 November 2012

reactivity is used for selective destruction of cancer cells, skin diseases, or the deactivation of blood-borne pathogens [1, 5].

Photooxygenation of anthracenes has received particular attention in the last decades. Experimental [2, 6–15] and theoretical [13–20] efforts have been made to unveil the photophysics and photochemistry of anthracene endoperoxides. Particularly interesting is the fact that such systems have the rare ability to decompose (thermally [21] or photochemically [6, 10, 12–15, 18, 22, 23]) via two different reaction pathways. In one pathway, homolytic cleavage of the peroxide O–O bond takes place, generating biradicals that evolve to quinone and diepoxide derivatives. The other pathway regenerates the parent hydrocarbon (in this case anthracene) and releases oxygen in the singlet state. Photochemically, these two paths are connected to different electronic states; this is commonly known as dual photochemistry. Cycloreversion and singlet oxygen generation occurs after an excitation to $\pi\pi^*$ states, while $\pi^*_{oo}\sigma^*_{oo}$ transitions (the antibonding π^*_{oo} orbital is occupied in this compound) are connected to the splitting of the O–O bond [14, 16–19, 24] and the rearrangement products. The existence of these two pathways has been however heavily questioned in the past. Several groups investigated the photolysis of aromatic endoperoxides under different experimental conditions, reaching different conclusions, and thus wondering about the nature of the first excited state [10, 13, 15]. In agreement with the early orbital analysis and state correlation diagrams of Kearns [16], the most recent femtosecond polarization resolved UV/IR pump-probe and steady-state fluorescence experiments combined with accurate excited state calculations showed that in anthracene-9,10-endoperoxide (APO, see Fig. 1), the S_1 state is of $\pi^*_{oo}\sigma^*_{oo}$ nature while higher states are of $\pi\pi^*$ character [18]. Further calculations discovered that the homolytic O–O cleavage in APO as well as in a smaller endoperoxide (cyclohexadieneendoperoxide, CHDEPO in Fig. 1) occurs through an eight-state degeneracy (four singlet and four triplet states) present in the potential energy surface [25–27]. This high-order degeneracy can be populated either thermally or photochemically from the electronic ground state and leads to a branching between the original reactant and the diradical rearrangement products [25].

In general, the absorption spectrum of endoperoxides is very broad and therefore theory is best suited to uncover its composition. Despite their structural similarity, not all endoperoxides necessarily have to show the same absorption spectrum and therefore the same photochemistry. In APO, the lowest singlet excited state S_1 has $\pi^*_{oo}\sigma^*_{oo}$ character and it leads to homolytic O–O cleavage while higher excited states, and in particular the S_4, seem to be responsible for cycloreversion [14]. In contrast, calculations in CHDEPO predict that the lowest excited state is a $\pi^*_{oo}\pi^*_{cc}$ excitation, directly connected to cycloreversion [26]. Experimentally, it has been seen that the homolytic O–O cleavage pathway in APO generates a biradical, which converts into electronically excited diepoxide [28]. Recently, the endoperoxide of mesodiphenylhelianthrene (MDHPO) has been investigated experimentally and it has been shown that it is non-fluorescent and that irradiation to the $\pi\pi^*$ band leads the corresponding diepoxide [11].

In an effort to extend our knowledge on the photophysics and photochemistry of endoperoxides from the theoretical point of view, in this paper, we investigate *o*-fluorine-phenyl-9-anthracene-9,10-endoperoxide **1** and its 9,10-bisarylanthracene analog **2**, see Fig. 1. These systems contain the APO core entity but also contain one or two phenyl groups, and therefore they are also related to MDHPO. Because the size of **2** is rather prohibitive to perform ab initio calculations, we use **1**, as a model system of the latter. The 9,10-bisarylanthracene system **2** is particularly interesting since it has been recently suggested as a molecular switch fueled by singlet oxygen [29]. The anthracene moiety serves as a stator and the phenyl substituted group is the rotor part which undergoes *cis*/*trans* isomerization. The rotation barrier is modulated by the presence or absence of oxygen [29].

To study the excited states of **1** and **2**, several methods have been employed. Time-dependent density functional theory (TD-DFT) is the logical choice for systems of large size; however, caution should be exercised when states showing charge transfer (CT) are present [30, 31]. Using APO as a reference case for which accurate MS-CASPT2/CASSCF (multi-state second-order perturbation theory on complete active space self-consistent-field) results were

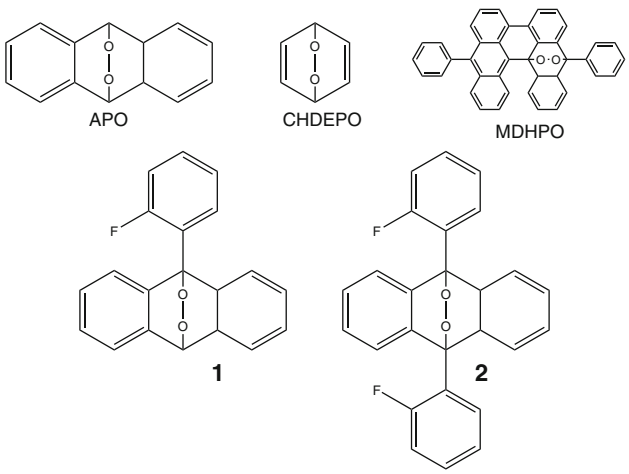

Fig. 1 Chemical formula of anthracene-9,10-endoperoxide (APO), cyclohexadieneendoperoxide (CHDEPO), mesodiphenylhelianthrene (MDHPO), *o*-fluorine-phenyl-9-anthracene-9,10-endoperoxide, **1**, and bis-*o*-fluorine-phenyl-9,10-anthracene-9,10-endoperoxide, **2**

available [18], a number of functionals belonging to the generalized gradient approximation (GGA), meta-GGA, global hybrids, and range-separated hybrid categories were tested by Corral et al. [20]. The outcome of that study was that functionals which contain an intermediate amount of exact exchange are best suited to describe simultaneously CT and local excitations in APO. The long-range corrected CAM-B3LYP functional and a functional denoted as B3LYP(32), combining 32 % of exact exchange, 72 % of non-local B88 exchange [32], and LYP [33] correlation, deliver the least average errors. Therefore, these functionals will be employed to calculate the excited states of **1**. As it will be shown, B3LYP(32) demonstrates the best performance, so that we shall employ this functional to calculate the excited states of the larger compound **2**. For comparison, the pure functional BP86 is also used in **1**.

The excited states of **1** are also calculated using the CC2 (second-order approximated coupled cluster) [34] method since this method should be able to provide good accuracy irrespectively of CT states. Finally, a more reliable description of the excited states of **1** is expected using multiconfigurational methods, such as, e.g., MS-CASPT2/CASSCF. Since the endoperoxide **1** is larger than APO, the application of CASSCF-based methods inevitably relies on choosing an active space suited to describe only a portion of the spectrum (see Sect. 2 for further details). An attractive alternative to CASSCF and CASPT2 is the use of RASSCF [35, 36] (restricted active space SCF) and its corresponding RASPT2 [37, 38]. The RASPT2/RASSCF approach allows extending the number of active orbitals by restricting the excitation level. Recently, it has been benchmarked in a number of molecules, pushing the field of photochemistry in a promising direction [37, 39, 40]. While in the CASSCF method the molecular orbital space is divided into three spaces (inactive, active, and empty), in RASSCF the active space is split in three further subspaces (RAS1, RAS2, and RAS3). The final wavefunction is obtained allowing a full configuration interaction expansion in the RAS2 (as in the active space of CASSCF) while restricting in RAS1 and RAS3 a predefined level of excitation, typically allowing up to singles (S), doubles (D), triples (T), or quadruples (Q). This additional flexibility allows studying systems which require larger active spaces; however, the different choices of configurational expansions make RASSCF less straightforward than CASSCF.

The main goal of this paper is to benchmark the excited states of **1** using RASPT2/RASSCF and compare the results with CASPT2/CASSCF, CC2, and TD-DFT results. TD-DFT is used to calculate the excited states of **2**. Since both molecules deliver a similar spectrum, we use **1** to go beyond the vertical absorption spectrum and obtain some insight into the photochemistry. Specifically, we compute the photochemical path corresponding to homolytic O–O cleavage in **1** and since this process was correlated with a four-state CI (4CI) in APO and CHDEPO (recall Fig. 1), where besides four singlet states, also four triplet states are degenerate, we investigate the possibility of such high-order degeneracy in **1**.

2 Computational details

The ground state equilibrium geometry of **1** and **2** and the most relevant rotamers were optimized by means of DFT with the standard functional B3LYP [33, 41] and the 6-31G(d,p) double-ζ basis set [42], as implemented in the GAUSSIAN 09 program [43]. A harmonic frequency calculation at the same level of theory was done to confirm that the obtained stationary points are minima of the potential energy surface. These geometries are employed for all the subsequent single point calculations.

The Franck-Condon vertical excitation energies and oscillator strengths of the lowest singlet excited states of the lowest energy structure of **1** were investigated using three different approaches (TD-DFT, CC2, and multiconfigurational methods—as stated in the introduction), while the UV absorption spectrum of **2** is only investigated using TD-DFT. In **1**, first, the B3LYP(32) and CAM-B3LYPY [44] functionals are used, together with the pure functional BP86 [32, 45] for comparison. The BP86 vertical excitation energies were calculated employing the resolution of identity approximation [46] and the triple-ζ valence polarization [47] (TZVP) basis set, as implemented in the TURBOMOLE 5.8 suite of programs [48]. The B3LYP(32) and CAM-B3LYP functionals were used with the 6-31G(d,p) basis set as implemented in the GAUSSIAN 09 program [43]. Then, CC2 calculations have been carried out utilizing the TURBOMOLE 6.2 suite of programs [48] and applying the resolution of identity approximation in conjunction with the TZVP basis set. Additionally, state-of-the-art multiconfigurational calculations have been performed using the MS-CASPT2/CASSCF [49, 50] and MS-RASPT2/RASSCF [35–38] hierarchical methods, as implemented in the MOLCAS 7.4 suite of programs [51–54]. By MS-CASPT2/CASSCF (or MS-RASPT2/RASSCF), we mean that single point calculations at the MS-CASPT2 (MS-RASPT2) level of theory using the CASSCF (RASSCF) reference wavefunction have been carried out. These multiconfigurational calculations employed the atomic natural orbitals small basis set (ANO-S) [55], with the contractions C,N,O[3s2p1d]/H[2s1p]. The two-electron integrals have been generated within the Cholesky decomposition [56].

The use of multiconfigurational methods requires a choice of the active space. The full active space of **1** should contain at least 28 electrons in 26 orbitals. Such an active space

would be composed of (see Fig. 2) six pairs of π_{an}/π^*_{an} orbitals of the anthracene body, three pairs of π_{ph}/π^*_{ph} orbitals of the *o*-fluorine-phenyl moiety, the peroxide orbitals σ_{oo}, σ^*_{oo}, $\pi_{oo,}$ and π^*_{oo} and additionally two pairs of $\sigma_{co}/\sigma^*_{co}$ orbitals connecting the peroxide group with the anthracene body, which, as shown in Ref. 19, are required to assure $\pi - \sigma$ correlation. A CASSCF calculation with this active space in a molecule of this size is computationally unfeasible. Therefore, calculations will be planned excluding from the outset the lowest occupied π orbitals localized on the anthracene or the phenyl group and the highest unoccupied π^* counterparts. Then, two reduced active spaces, (14, 12) and (12, 12), were designed, similar to the ones employed in the calculation of the unsubstituted APO [18]. The CASSCF(14, 12) calculation comprises four pairs of π_{an}/π^*_{an} orbitals and all peroxide orbitals σ_{oo}, σ^*_{oo}, π_{oo}, and π^*_{oo}. This active space is best suited to describe excitations within the peroxide bridge, within the anthracene body, and the corresponding CT states. The smaller CASSCF(12, 12) calculation includes the four pairs of π_{an}/π^*_{an} orbitals and additionally two pairs of π_{ph}/π^*_{ph} orbitals, allowing for the description of some of the transitions taking place within the whole aromatic π-system, including the phenyl group (see Fig. 2). Both active spaces exclude the two pairs of $\sigma_{co}/\sigma^*_{co}$ orbitals to save computational time.

In addition to CASSCF, RASSCF calculations have been performed. Since RASSCF allows including a large number of orbitals distributed in three RAS subspaces, it seems the natural tool to benchmark the excited states of **1**. The RAS1 includes typically orbitals with large occupation numbers. In these orbitals, a maximum number of electron holes is allowed. Accordingly, the RAS3 is constructed from virtual orbitals with small occupation numbers and here only a maximum number of electrons is allowed. The RAS2 is equivalent to the active space of the CASSCF methodology, where all possible configurations are taken into account. A wise choice of the different RAS subspaces can reduce drastically the number of configuration state functions (CFSs) and therefore the computational cost while delivering accurate results, which in turn allows increasing the size of the active space. In order to label the RAS calculations, the notation RAS(*n, l, m; i, j, k*) of Gagliardi and coworkers [39] is adopted. The index *n* labels the number of active electrons, *l* the maximum number of holes in the RAS1 and *m* the maximum number of electrons in the RAS3. The labels *i, j*, and *k* state the number of active orbitals in the RAS1, RAS2, and RAS3, respectively.

After extensive testing, the calculation of **1** has been done with a RASSCF(22, 2, 2; 8, 6, 6) partition, see Fig. 2. The RAS2 contains only the two peroxide orbitals (π^*_{oo} and σ^*_{oo}) involved in the $\pi^*_{oo}\sigma^*_{oo}$ state and two additional pairs of π_{an}/π^*_{an} orbitals. Accordingly, the RAS1 includes the rest of the occupied orbitals: two σ_{co}, two peroxide (σ_{oo} and π_{oo}), two π_{ph} and two π_{an} orbitals. The RAS3 consists of the antibonding analogs to the σ_{co}, π_{ph} and π_{an} orbitals. This partition spans over a reference space of more than 700 000 CFSs. In this calculation, a maximum number of two holes in the RAS1 and two electrons in the RAS3 were allowed, that is, only S and D excitations are considered, since higher levels of excitation are computationally unfeasible and should not affect the excitation energies by more than 0.1 eV [39].

All the CASSCF and RASSCF wavefunctions are obtained through state-average (SA) calculations with equal weights. To improve the energies, in all cases, dynamical correlation was included by performing MS-CASPT2 [50] or MS-RASPT2 [37] using a zeroth-order Hamiltonian containing a standard IPEA shift of 0.25 a.u. In order to prevent effects from intruder states, a level shift [57] of 0.3 a.u. was added to the zeroth-order Hamiltonian, as in Ref. 18. The oscillator strengths have been calculated at the MS-CASPT2 and MS-RASPT2 levels of theory with the CAS state interaction method [58].

In order to find out whether a 4CI is also present in **1**, we follow the same procedure adopted in Ref. 25. First, a two-state degeneracy (a CI) is optimized following the minimum energy path (MEP) from the lowest S_1 state. A MEP or intrinsic reaction coordinate (IRC) is the steepest descent minimum energy reaction pathway calculated in mass-weighted coordinates. Since a MEP consists of a series of geometry optimizations, each requiring the minimization of the potential energy on a hyperspherical cross-section of the PES centered on a given reference geometry and characterized by a predefined radius [51], and this is computationally demanding, an smaller active space, only containing the relevant orbitals located in the endoperoxide group is employed. The resulting active space contains six electrons in four orbitals (σ_{oo}, π_{oo}, π^*_{oo}, σ^*_{oo}), denoted by SA2-CASSCF(6,4). At the optimized CI geometry, two SA4-CASSCF(6,4) calculations, refined at MS-CASPT2 level of theory, were carried out to inspect the energy of the four lowest singlet and four lowest triplet states, respectively. The possibility of intersystem crossing (ISC), that is, a transition between the singlet to the triplet states, at this geometry was investigated by calculating the spin-orbit couplings (SOCs) between the eight states at the CASSCF level of theory. The SOCs are calculated using the two-component Douglas–Kroll–Hess Hamiltonian [59], as implemented in the Molcas package [51].

3 Results

3.1 Ground states geometries

The rotation of the *o*-fluorine-phenyl moiety in **1** gives rise to four different minima: a *trans*, a *cis*, and two symmetric

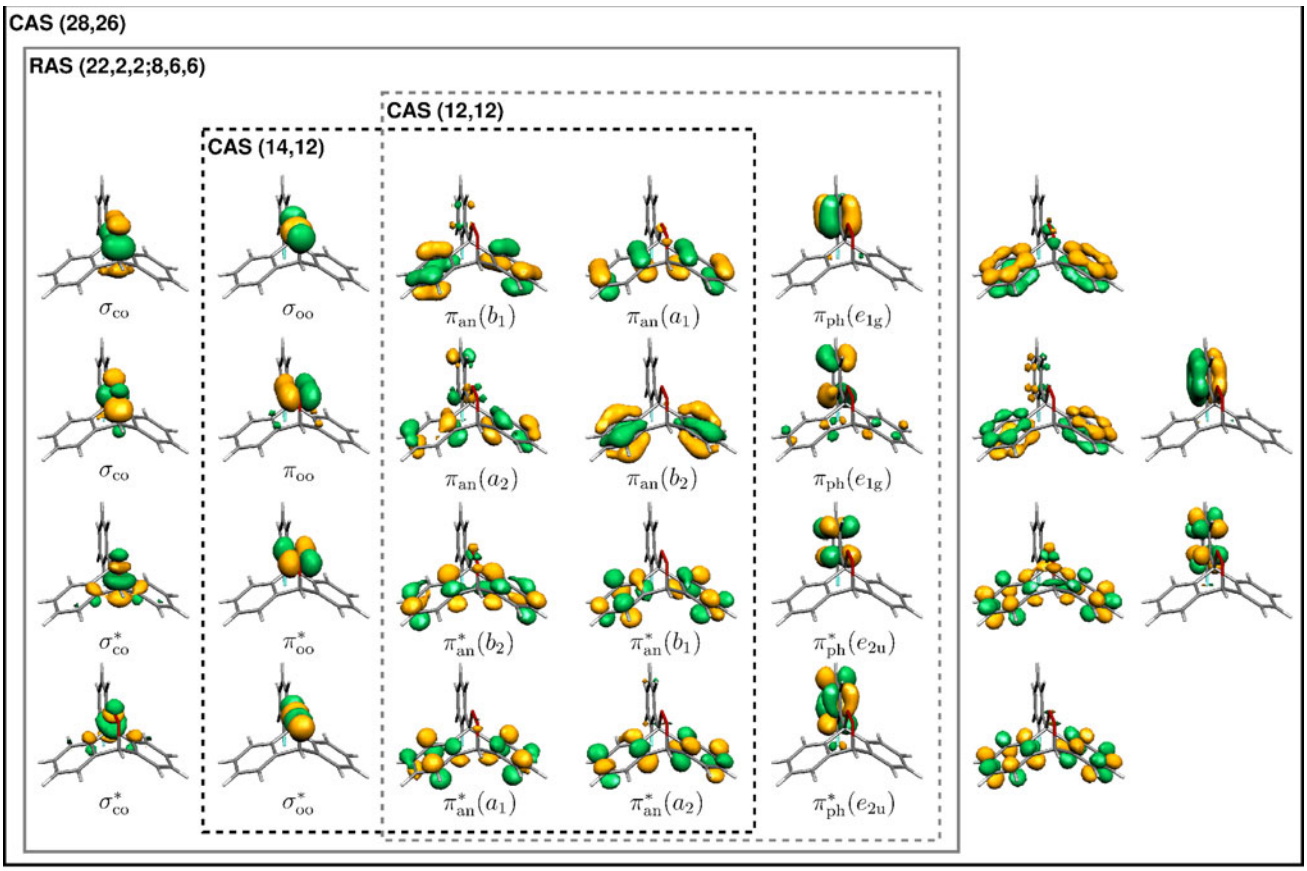

RAS (22,2,2;8,6,6)							
RAS1				RAS2		RAS3	
σ_{co}	σ_{co}	σ_{oo}	π_{oo}	π^*_{oo}	σ^*_{oo}	σ^*_{co}	σ^*_{co}
$\pi_{an}(a_1)$	$\pi_{an}(b_2)$			$\pi_{an}(b_1)$	$\pi^*_{an}(b_2)$	$\pi^*_{an}(a_2)$	$\pi^*_{an}(b_1)$
$\pi_{ph}(e_{1g})$	$\pi_{ph}(e_{1g})$			$\pi_{an}(a_2)$	$\pi^*_{an}(a_1)$	$\pi^*_{ph}(e_{2u})$	$\pi^*_{ph}(e_{2u})$

Fig. 2 Molecular orbitals for a CASSCF(28,26) (*solid black frame*), RASSCF(22, 2, 2; 8, 6, 6,) (*solid gray*), CASSCF(14, 12) (*dashed black*) and CASSCF(12, 12) (*dashed gray*) calculations. The orbitals localized on the anthracene (an) or on the phenyl (ph) groups are further labeled with a symmetry tag from the local C_{2v} or D_{6h} point group, respectively

gauche isomers. The *trans*-conformation (Fig. 3a) is the global minimum and only this will be used to calculate the excited states. The *cis*- (Fig. 3c) and two equivalent *gauche*-rotamers (Fig. 3b) are only 4.4 and 7.4 kcal/mol higher in energy, respectively, and separated by transition states located at ca. 9 kcal/mol (not shown). The geometries of all the structures are very similar, in particular the O–O bond length is hardly affected by rotation. The orientation of the geometry was chosen so that the *o*-flourin-phenyl moiety and the peroxide bridge are located in the xz-plane. Although this structure belongs to the C_s point group, the excited state calculations were all performed without symmetry, unless otherwise specified. Yet, a C_s symmetry tag has been attached to the calculated states.

In **2**, the rotation of both *o*-fluorine-phenyl moieties give raise to one *trans–trans* (Fig. 3d), one *cis–cis* (Fig. 3f), two equivalent *cis–trans* (Fig. 3e), and two pairs of equivalent *gauche–trans* and *gauche-cis*, as well as four *gauche–gauche* isomers (not shown). Following the knowledge gained with **1**, the *gauche* structures were assumed to be higher in energy and hence were not calculated. From the *cis*/*trans* structures, the most stable one is the *trans–trans* structure, analogously to the *trans*-isomer of **1**. The isomers of compound **2** display slightly more pronounced changes in the endoperoxide bond length, but resemble in the scaffolding the structures of **1**.

3.2 Electronic excited states

First, we shall discuss the performance of the more economic TD-DFT methods. In Table S1 of the Supporting Information, a full account of the vertical excitation energies, oscillator strengths, and electronic character of the first ten singlet excitations of **1** obtained with the BP86,

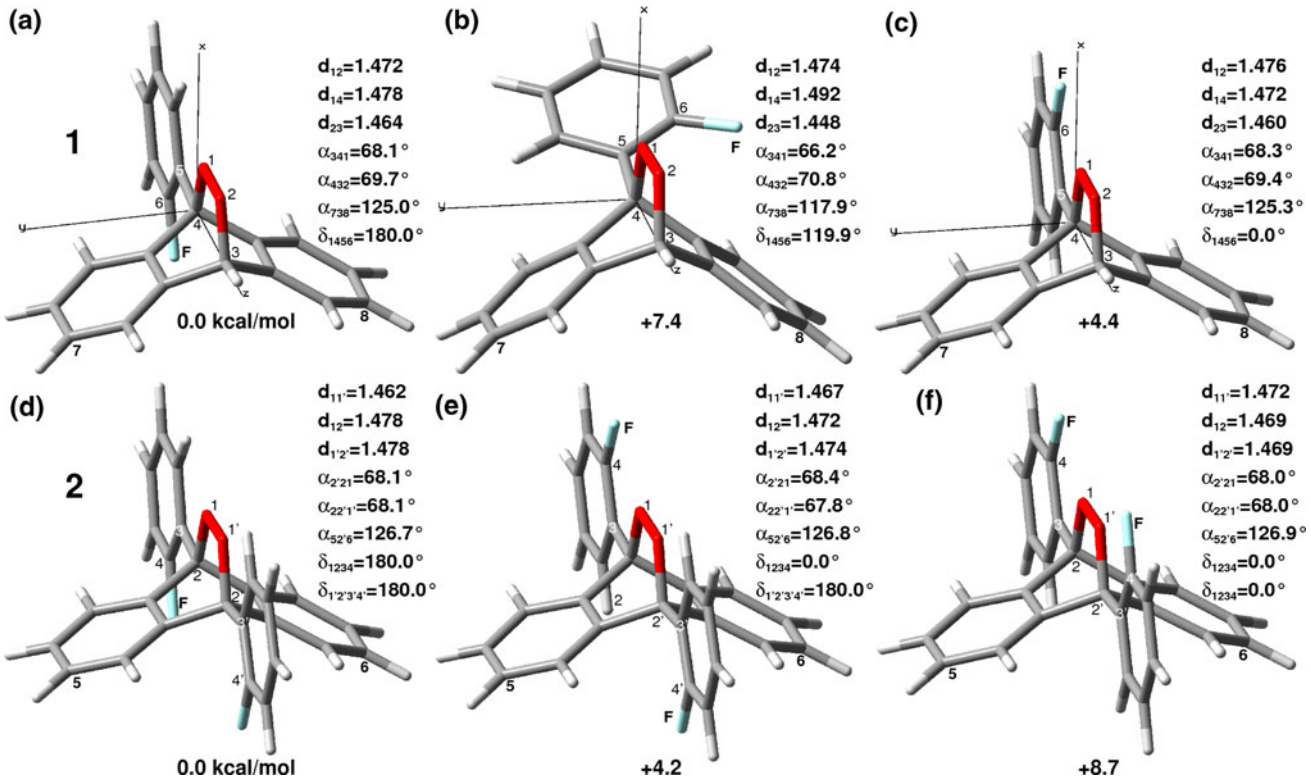

Fig. 3 Different rotamers of endoperoxides **1** and **2**: *Trans* (**a**), *gauche* (**b**), *cis* (**c**), *trans–trans* (**d**), *cis–trans* (**e**), and *cis–cis* (**f**). Geometries and relative energies (in kcal/mol) are obtained at B3LYP/6-31G(d, p) level of theory. Distances in Ångströms and angles in degrees

CAM-B3LYP, and B3LYP(32) functionals is given. In Table 1, we only summarize the results obtained with the B3LYP(32) functional for **1** and **2**.

The pure BP86 functional predicts the $\pi^*_{oo}\sigma^*_{oo}$ state of **1** as the ninth excited state at 4.36 eV, with an oscillator strength of 0.0043. Misleadingly, these values are even in reasonable agreement with the CASPT2 and RASPT2 ones (see below); however, seven spurious CT states of either $\pi^*_{oo}\pi^*_{an}$ (S_1, S_3, S_5, S_7), $\pi^*_{oo}\pi^*_{ph}$ (S_2, S_4), or $\pi_{an}\pi^*_{ph}$ (S_8) character precede the $\pi^*_{oo}\sigma^*_{oo}$ state; (contributions in the anthracene or phenyl moiety are denoted as an and ph, respectively). Furthermore, one $\pi_{an}\pi^*_{an}$ (S_6) state is also wrongly intercalated among the CT states. The tendency of pure functionals to strongly underestimate the energy of the CT states is well known [31] and should therefore not surprise. This calculation only emphasizes that the wrong choice of functionals can lead to unphysical results, which in this particular case can be catastrophic to interpret the by itself difficult and controversial localization of the first excited state of endoperoxides [11].

CAM-B3LYP and B3LYP(32), in contrast to BP86, give more physical results, very similar to each other. Both functionals assign the S_1 state as a $\pi^*_{oo}\sigma^*_{oo}$ transition, although the wavefunction also shows other small contributions. This state (of 1A″ character) is predicted at an energy of about 4.6 eV with a very weak oscillator strength. The next five states are very close to each other within 0.3 eV and correspond to $\pi_{an}\pi^*_{an}$, $\pi_{ph}\pi^*_{ph}$ and CT states. Although some transitions are described similarly with CAM-B3LYP and B3LYP(32), the details are different. Moreover, CAM-B3LYP predicts energies ca. 0.4 eV blueshifted with respect to B3LYP(32). If we take the RASPT2 energy of the $\pi^*_{oo}\pi^*_{an}$ state (discussed later) as a reliable landmark, the energies of the CT states provided by the B3LYP(32) functional are better than those of CAM-B3LYP.

The second excited state is the 2A″ and B3LYP(32) assigns it (see Table 1) as pure π_{an} π^*_{an} transitions. The S_3 or 3A″ state is very close to the 2A″ but it is a mixture of localized transitions in the anthracene, in the endoperoxide group, and CT. The 4A″ state is the first state displaying aromatic transitions involving the phenyl group and it also shows the counterpart of the mixing with the $\pi^*_{oo}\sigma^*_{oo}$ transition found in the 1A″ and 3A″ states. While the next excited state, 2A′ corresponds again to pure π_{an} π^*_{an} transitions, the rest of the states are different combinations of local and CT excitations.

Interestingly, the excited states of **2** calculated with B3LYP(32) (for MOs see Figure S1 of the Supporting Information) are very similar to those of **1**. The first excited

Table 1 B3LYP(32) calculation for **1**(left) and **2**(right)

B3LYP(32)										
1						**2**				
State		ΔE/eV	f	Character	c^2/%	State	ΔE/eV	f	Character	c^2/%
1A″	(1A″)	4.57	0.0001	$\pi^*_{oo}\sigma^*_{oo}$	42	1A″	4.65	0.0000	$\pi^*_{oo}\sigma^*_{oo}$	33
				$\pi^*_{oo}\pi^*_{an}(b_2)$	37				$\pi^*_{oo}\pi^*_{an}(b_2)$	32
				$\pi_{ph}(e_{1g})\ \sigma^*_{oo}$	11				$\pi_{ph}(a_2)\ \sigma^*_{oo}$	15
									$\pi_{ph}(a_2)\pi^*_{an}(b_2)$	10
2A″	(2A″)	5.18	0.0004	$\pi_{an}(b_1)\pi^*_{an}(b_2)$	75	2A″	5.20	0.0000	$\pi_{an}(b_1)\pi^*_{an}(b_2)$	94
				$\pi_{an}(b_1)\pi^*_{an}(a_1)$	8					
3A″	(4A″)	5.19	0.0005	$\pi_{an}(b_1)\pi^*_{an}(a_1)$	27	3A″	5.21	0.0001	$\pi_{an}(b_1)\pi^*_{an}(a_1)$	40
				$\pi^*_{oo}\pi^*_{an}(b_2)$	23				$\pi^*_{oo}\pi^*_{an}(b_2)$	23
				$\pi_{an}(b_1)\pi^*_{an}(b_2)$	19				$\pi_{an}(a_2)\pi^*_{an}(b_2)$	16
				$\pi^*_{oo}\sigma_{oo}{}^*$	13					
4A″	(3A″)	5.30	0.0090	$\pi^*_{oo}\pi^*_{an}(b_2)$	22	4A″	5.38	0.0061	$\pi^*_{oo}\pi^*_{an}(b_2)$	24
				$\pi^*_{oo}\sigma_{oo}{}^*$	19				$\pi_{an}(a_2)\pi^*_{an}(b_2)$	23
				$\pi_{ph}(e_{1\ g})\pi^*_{an}(b_2)$	17				$\pi^*_{oo}\ \sigma_{oo}{}^*$	20
				$\pi_{an}(b_1)\pi^*_{an}(a_1)$	16				$\pi_{ph}(a_2)\pi^*_{an}(b_2)$	10
				$\pi_{an}(a_2)\pi^*_{an}(b_2)$	15				$\pi_{ph}(a_2)\sigma^*_{oo}$	9
2A′	(2A′)	5.44	0.0034	$\pi_{an}(b_2)\pi^*_{an}(b_2)$	50	2A′	5.43	0.0031	$\pi_{an}(b_2)\pi^*_{an}(b_2)$	51
				$\pi_{an}(a_1)\pi^*_{an}(a_1)$	16				$\pi_{an}(b_1)\pi^*_{an}(b_1)$	19
				$\pi_{an}(b_1)\pi^*_{an}(b_1)$	14				$\pi_{an}(a_1)\pi^*_{an}(a_1)$	15
3A′	(3A′)	5.51	0.0218	$\pi_{ph}(e_{1\ g})\ \pi^*_{ph}(e_{2u})$	28	3A′	5.50	0.0503	$\pi_{ph}(b_1)\pi^*_{ph}(a_2)$	28
				$\pi_{an}(a_2)\pi^*_{ph}(e_{2u})$	22				$\pi^*_{oo}\pi^*_{ph}(b_1)$	17
				$\pi_{ph}(e_{1\ g})\ \pi^*_{ph}(e_{2u})$	21				$\pi_{ph}(a_2)\pi^*_{ph}(b_1)$	14
				$\pi^*_{oo}\pi^*_{ph}(e_{2u})$	20				$\pi_{ph}(b_1)\pi^*_{ph}(a_2)$	14
									$\pi_{ph}(a_2)\pi^*_{ph}(b_1)$	11
5A″	(5A″)	5.67	0.0002	$\pi^*_{oo}\pi^*_{an}(a_1)$	86	4A′	5.51	0.0019	$\pi_{ph}(b_1)\pi^*_{ph}(b_1)$	29
				$\pi_{ph}(e_{1g})\pi^*_{an}(a_1)$	10				$\pi^*_{oo}\pi^*_{ph}(a_2)$	15
									$\pi_{ph}(b_1)\pi^*_{ph}(b_1)$	15
									$\pi_{ph}(a_2)\pi^*_{ph}(a_2)$	14
									$\pi_{ph}(a_2)\pi^*_{ph}(a_2)$	11
4A′	–	5.82	0.0019	$\pi_{an}(b_1)\pi^*_{ph}(e_{2u})$	83	5A″	5.77	0.0000	$\pi^*_{oo}\pi^*_{an}(a_1)$	77
				$\pi^*_{oo}\pi^*_{ph}(e_{2u})$	10				$\pi_{ph}(a_2)\pi^*_{an}(a_1)$	10
									$\pi_{an}(a_2)\pi^*_{an}(a_1)$	10
5A′	–	5.90	0.0211	$\pi^*_{oo}\pi^*_{ph}(e_{2u})$	62	5A′	5.78	0.0005	$\pi_{an}(b_1)\pi^*_{ph}(b_1)$	92
				$\pi_{ph}(e_{1g})\ \pi^*_{ph}(e_{2u})$	14					
				$\pi_{an}(b_1)\pi^*_{ph}(e_{2u})$	14					
6A″	–	5.97	0.0002	$\pi_{ph}(e_{1g})\ \pi^*_{an}(b_2)$	53	6A′	5.79	0.0020	$\pi_{an}(b_1)\pi^*_{ph}(a_2)$	91
				$\pi_{an}(a_2)\pi^*_{an}(b_2)$	33					

The states are labeled according to the C_s symmetry (in parenthesis the RASPT2 assignment for **1**). Excitation energies ΔE (in eV), oscillator strengths f, and leading configurations obtained by the indicated electron replacement with their weight (c^2)

state is located at 4.65 eV and corresponds to an excitation within the endoperoxide group (although the $\pi^*_{oo}\pi^*_{an}$ contribution has a similar weight). All the nine following excited states are congested within 1 eV and correspond to combinations of $\pi_{an}\pi^*_{an}$, $\pi_{ph}\pi^*_{ph}$ and CT states. In general, both **1** and **2** seem to have a very similar UV absorption spectrum when considering the energies, oscillator strengths, and composition of the wavefunctions. We are therefore confident that they should be very similar in their photochemical behavior. Accordingly, in the following, we shall only use **1** for further validation of the excited states and inspection of its PES.

Next, we discuss the results of the MS-CASPT2/CASSCF calculations with the two active spaces; these are

Table 2 MS-CASPT2/CASSCF calculation for 1

State	Active space (14, 12) (CSFs: 169884)					Active space (12, 12) (CSFs: 113616)				
	ΔE/eV		f	Character	c^2/%	ΔE/eV		f	Character	c^2/%
	CASSCF	MS-CASPT2				CASSCF	MS-CASPT2			
1A″	5.53	4.81	0.0029	$\pi^*_{oo}\sigma^*_{oo}$	70					
2A″	6.04	5.22	0.0028	$\pi_{an}(b_1)\pi^*_{an}(a_1)$	15	6.31	4.95	0.0004	$\pi_{an}(b_1)\pi^*_{an}(a_1)$	30
				$\pi_{an}(b_1)\pi^*_{an}(b_2)$	14				$\pi_{an}(a_2)\pi^*_{an}(b_2)$	27
				$\pi_{an}(a_1)\pi^*_{an}(b_1)$	11					
2A′	6.20	5.48	0.0001	$\pi_{an}(b_1)\pi^*_{an}(b_1)$	21	6.29	5.39	0.0003	$\pi_{an}(b_2)\pi^*_{an}(b_2)$	22
				$\pi_{an}(b_2)\pi^*_{an}(b_2)$	11				$\pi_{an}(b_1)\pi^*_{an}(b_1)$	20
									$\pi_{an}(a_1)\pi^*_{an}(a_1)$	14
									$\pi_{an}(a_2)\pi^*_{an}(a_2)$	12
4A″						7.57	5.47	0.0019	$\pi_{an}(b_1)\pi^*_{an}(b_2)$	77
3A′						6.24	5.55	0.0036	$\pi_{ph}(e_{1g})\pi^*_{ph}(e_{2u})$	41
									$\pi_{ph}(e_{1g})\pi^*_{ph}(e_{2u})$	27
A″						8.68	6.37	1.2091	$\pi_{an}(a_2)\pi^*_{an}(b_2)$	42
									$\pi_{an}(b_1)\pi^*_{an}(a_1)$	38
A″						8.81	6.42	0.0001	$\pi_{an}(a_2)\pi^*_{an}(a_1)$	66
									$\pi_{an}(b_2)\pi^*_{an}(b_1)$	13

The states are labeled according to C_s symmetry. Excitation energies ΔE (in eV), oscillator strengths f, and leading configurations obtained by the indicated electron replacement with their weight (c^2), computed with the active spaces (14, 12) and (12, 12). The number of CFSs refers to those spanned by the CASSCF wavefunction

summarized in Table 2. Recall that the (14, 12) active space, see Fig. 2, is tailored to describe primarily the excited states which involve the endoperoxide group. According to the SA4-CASSCF(14, 12) calculation, the first excited state is of symmetry A″ (henceforth labeled 1A″) and has an excitation energy of 5.53 eV. Analysis of the orbitals reveals that it corresponds to a $\pi^*_{oo}\sigma^*_{oo}$ transition and therefore direct irradiation to this state should lead to O–O homolytic dissociation. In passing, we note that this result confirms that the B3LYP(32) and CAM-B3LYP functionals are correct in their assignment, in contrast to BP86. At the CASSCF level of theory, the next two states are close in energy and have a multiconfigurational wavefunction with different participating excitations within the anthracene moiety, $\pi_{an}\pi^*_{an}$ (only configurations with more than 10 % are shown). According to the symmetry of the orbitals involved in the transition, these states correspond to the 2A″ and 2A′ states, respectively. The inclusion of dynamical correlation via MS-CASPT2 redshifts the energies by $0.7 - 0.8$ eV but respects the order of the states. All these three computed states are weak absorbing or basically dark, with oscillator strengths ranging from 0.0001 to 0.0029. In comparison with the B3LYP(32) results, the latter underestimate by ca. 0.25 eV the 1A″ state and by less than 0.05 eV the 2A″ and 2A′ states. In this way, the agreement between both methods, B3LYP(32) and MS-CASPT2 for these selected transitions is very satisfactory.

Other transitions, for instance, those involving $\pi\pi^*$ excitations should be better investigated with the (12, 12) active space, see Fig. 2. While this active space is capable to describe excitations within the aromatic π-system (π_{an} and π_{ph}), it cannot account for intraperoxide states and CT states such as $\pi^*_{oo}\pi^*_{an}$ or $\pi^*_{oo}\pi^*_{ph}$. Using this active space, a calculation without symmetry (similar to the one with the (14, 12)) has been carried out. Unfortunately, the active space is too small for such intent and led to states with spurious mixed symmetry, which we do not report here. To palliate this problem, another calculation with C_s symmetry, averaged over three and four states of A′ and A″ symmetry, respectively, has been performed. The results are compiled in Table 2. The first and second excited states of this calculation can be assigned as the 2A″ and 2A′ states obtained with the (14, 12) active space. Both states involve excitations located in the anthracene group. The obtained CASSCF and MS-CASPT2 excitation energies differ by 0.1-0.2 eV from those obtained with (14, 12); such differences are a consequence of the different averaging of number of roots. As a consequence, the gap between the second and third excited states predicted by ca. 0.2 eV with the (14, 12) active space has almost doubled in the (12, 12) calculation and these two states are redshifted. The remaining states obtained with this active space are not present in the (14, 12) calculation. The next state higher in energy is also an excitation within the anthracene group and has A″ symmetry. This state is labeled as 4A″ since as

it will be seen later, the 3A″ is missing in this CASSCF calculation. The following state predicted at 5.55 eV (MS-CASPT2) is the 3A′ and involves electronic excitations within the phenyl group. The remaining two states are of A″ symmetry and have not been numbered because the following calculations will show that some preceding states are not described with this too small active space.

Generally speaking, the results obtained with both active spaces can be seen as complementary to each other. The 2A″ and 2A′ states are both obtained with CASSCF(14, 12) and CASSCF(12, 12) while the 1A″ state is only predicted with CASSCF(14, 12). Higher states located in the anthracene and phenyl groups are only obtained with CASSCF(12, 12), but they are also conditioned by the orbitals included in the active space and their assignment is troublesome if one is lacking another trustable reference to compare with. Clearly, it would be more convenient to have a method that can describe all states simultaneously with the same accuracy, or at least the most relevant ones. RASSCF calculations are the natural remedy to palliate the deficiency of reduced active spaces, although they still rely on a manual choice of the orbitals involved in each partition.

Table 3 shows the results obtained with RASSCF (22,2,2;8,6,6) and RASPT2, averaged over six states. All excitations that result from the orbitals included in the RAS2 space belong to A″. The A′ states result only from excitations from the spaces RAS1 and RAS3. This means that x-polarized transitions are calculated more accurately than those polarized in the yz-plane. Therefore, not surprisingly, all five lowest excited states predicted by this RASSCF calculation belong to A″ symmetry. Hence, this RASSCF calculation cannot describe either all the excitations of the absorption spectrum simultaneously with the same accuracy. However, since the local excitation at the O–O bridge, which is the key point of this investigation, is of A″ character and the majority of the lowest excited states belongs to A″ symmetry (as also shown by the CC2 and B3LYP(32) calculations), the sacrifice on the quality of the A′ subspace can be justified. Unfortunately, a calculation including all anthracene orbitals in the RAS2 and thus being able to describe the A″ and A′ states on the same footing is not currently feasible on our computers.

As one can see, the lowest excited state, 1A″, has a large contribution from $\pi^*_{oo}\sigma^*_{oo}$ excitation, as in the CASSCF calculation (Table 2), but now the wavefunction shows a mixing with the $\pi^*_{oo}\pi^*_{an}$ CT state, as did the B3LYP(32) wavefunction (Table 1). As a consequence of this mixing, the corresponding oscillator strength is weaker than that predicted with CASSCF alone. The absorption energy predicted by RASSCF is 5.88 eV and as it is usual upon introduction of electronic correlation, RASPT2 stabilizes the state until 4.44 eV, in close agreement with the value of 4.57 eV of B3LYP(32). The comparison between CASPT2 and RASPT2 shows that the state is redshifted from 4.81 eV (CASPT2) until 4.44 eV (RASPT2).

Table 3 MS-RASPT2/RASSCF calculation for 1

Configurational space (22, 2, 2; 8, 6, 6) (CSFs: 709471)					
State	ΔE/eV		f	Character	c^2/%
	RASSCF	MS-RASPT2			
1A″	5.88	4.44	0.0002	$\pi^*_{oo}\sigma^*_{oo}$	45
				$\pi^*_{oo}\pi^*_{an}(b_2)$	37
2A″	6.95	5.05	0.0865	$\pi_{an}(b_1)\pi^*_{an}(a_1)$	31
				$\pi_{an}(b_1)\pi^*_{an}(b_2)$	24
				$\pi_{an}(a_2)\pi^*_{an}(b_2)$	17
3A″	6.72	5.14	0.0004	$\pi_{an}(a_2)\pi^*_{an}(b_2)$	29
				$\pi^*_{oo}\pi^*_{an}(b_2)$	28
				$\pi^*_{oo}\sigma^*_{oo}$	23
4A″	7.18	5.36	0.0164	$\pi_{an}(b_1)\pi^*_{an}(b_2)$	28
				$\pi_{an}(b_1)\pi^*_{an}(a_1)$	18
				$\pi^*_{oo}\pi^*_{an}(b_2)$	13
				$\pi^*_{oo}\sigma^*_{oo}$	11
5A″	7.60	5.60	0.0004	$\pi^*_{oo}\pi^*_{an}(a_1)$	80

The states are labeled according to C_s symmetry. Excitation energies ΔE (in eV), oscillator strengths f, and leading configurations obtained by the indicated electron replacement with their weight (c^2). The number of CFSs refers to those spanned by the RASSCF wavefunction

Higher excitations have all $\pi\pi^*$ character, as predicted by the CASPT2/CASSCF but the details are different. The 2A″, 3A″, and 4A″ states result from $\pi_{an}\pi^*_{an}$ excitations but 3A″ and 4A″ have also CT contributions, not present in any of the CASSCF calculations. The 5A″ state is also a CT state that was not possible to obtain with the (12, 12) active space (recall Table 2). It is interesting that the local $\pi^*_{oo}\sigma^*_{oo}$ excitation is also mixed within the 3A″ and 4A″ excited states, as it was found at B3LYP(32) level of theory. A careful comparison of the contributing excitations reveals that the S_4 or 4A″ of B3LYP(32) corresponds to the 3A″ of RASPT2.

Looking at the oscillator strengths, it can be concluded that RASSCF clearly predicts the 2A″ to be the spectroscopic state of **1**, with an oscillator strength of 0.09, and corresponding to pure local excitations within the anthracene moiety. Surprisingly, this excitation was very weak with B3LYP(32) or any other from the functionals tried (see Table S1). The rest of the states containing $\pi^*_{oo}\pi^*_{an}$ CT contributions are very weakly absorbing. CT excitations involving the phenyl moiety were not found within the first six A″ states. Presumably, they are located at higher excitation energies, which are not accessible with the current number of roots.

Since CC2 is independent of choices for active orbitals, we found it interesting to perform such a calculation on **1**.

As shown in Table 4, the calculation of 10 states delivers 5 states of A′ and A″ symmetry, from which the lowest three (S_1–S_3) correspond to the 1A″–3A″ obtained with RAS-SCF/RASPT2. In general, the CC2 results are in reasonable agreement with the RASPT2 data. The first excited state is located at 4.29 eV, in close agreement with RASPT2 (4.44 eV) and B3LYP(32) (4.57 eV). It is composed of two main transitions: the $\pi^*_{oo}\sigma^*_{oo}$ and the $\pi^*_{oo}\pi^*_{an}$ excitations. However, an important difference with the RASPT2 and B3LYP(32) calculation is that the $\pi^*_{oo}\sigma^*_{oo}$ transition has only a minor weight, while the $\pi^*_{oo}\pi^*_{an}$ predominates. Its oscillator strength of 0.0025 is in range of the corresponding CASPT2 and RASPT2 values. The next two excited states of A′ and three of A″ symmetry are within 0.2 eV and can be directly assigned to those obtained with RASPT2 (A″) and CASPT2 (A′), see assignment in parenthesis in Table 4. These five states are of π_{an}-π^*_{an}, $\pi_{ph}\pi^*_{ph}$, and $\pi^*_{oo}\pi^*_{an}$ character. The wavefunction of 3A″ is the counterpart of the 1A″ one, showing a significant $\pi^*_{oo}\sigma^*_{oo}$ contribution. The 5A″ state, at 5.45 eV is dark and corresponds to a local excitation within the anthracene moiety. Until here, the order of all the states is preserved with respect to RASPT2 and CASPT2 except for the fourth and fifth states of A″ symmetry, which are altered by CC2 excitation. In general, the energies of the A″ states are less than 0.2 eV underestimated compared to RASPT2. After the 5A″ state, CC2 predicts three states of A′ with CT character from the endoperoxide bridge to the anthracene or phenyl moieties: either $\pi^*_{oo}\pi^*_{an}$ or $\pi^*_{oo}\pi^*_{ph}$, which cannot be found mirrored in any of the multiconfigurational calculations performed. Worth to mention is that the D1 multireference diagnostic in the CC2 calculation gives a value of 0.0637; hence, the ground state is not well described by a single determinantal reference wavefunction and the obtained results are also to take with caution.

Table 4 CC2 calculation for 1

CC2					
State		ΔE/eV	f	Character	c^2/%
1A″	(1A″)	4.29	0.0025	$\pi^*_{oo}\pi^*_{an}(b_2)$	65
				$\pi^*_{oo}\sigma^*_{oo}$	18
2A″	(2A″)	4.95	0.0013	$\pi_{an}(b_1)\pi^*_{an}(a_1)$	37
				$\pi_{an}(a_2)\pi^*_{an}(b_2)$	28
3A″	(3A″)	5.11	0.0094	$\pi^*_{oo}\sigma^*_{oo}$	37
				$\pi^*_{oo}\pi^*_{an}(b_2)$	20
2A′	(2A′)	5.12	0.0025	$\pi_{an}(b_2)\pi^*_{an}(b_2)$	38
				$\pi_{an}(a_1)\pi^*_{an}(a_1)$	19
				$\pi_{an}(b_1)\pi^*_{an}(a_2)$	15
4A″	(5A″)	5.15	0.0004	$\pi^*_{oo}\pi^*_{an}(a_1)$	84
3A′	(3A′)	5.15	0.0169	$\pi_{ph}(e_{1g})\pi^*_{ph}(e_{2u})$	59
				$\pi_{ph}(e_{1g})\pi^*_{ph}(e_{2u})$	28
5A″	(4A″)	5.45	0.0000	$\pi_{an}(b_1)\pi^*_{an}(b_2)$	84
4A′	–	5.55	0.0123	$\pi^*_{oo}\pi^*_{ph}(e_{2u})$	80
5A′	–	5.86	0.0049	$\pi^*_{oo}\pi^*_{ph}(e_{2u})$	55
				$\pi^*_{oo}\pi^*_{an}(b_1)$	24
6A′	–	5.88	0.0035	$\pi^*_{oo}\pi^*_{an}(b_1)$	86

The states are labeled according to the C_s symmetry (in parenthesis the RASPT2 assignment). Excitation energies ΔE (in eV), oscillator strengths f, and leading configurations obtained by the indicated electron replacement with their weight (c^2)

In general, the application of the three methods (B3LYP(32), CC2, and CASPT2/RASPT2) illustrates that none of the employed methods give a complete satisfactory answer and a straightforward assignment of the electronic excited states is difficult. In particular, the nature of the first excited state cannot be ambiguously characterized. While CASPT2 seems to indicate that the S_1 is predominantly a $\pi^*_{oo}\sigma^*_{oo}$ transition and should thus lead exclusively to O–O splitting, this assignment is less clear when using RASPT2 and B3LYP(32), since the contribution from $\pi^*_{oo}\pi^*_{an}$ increases, and it is even reversed with CC2, where the latter contribution has the greatest weight. It is fair to note that a similar trend was found in APO [18, 20]. However, in that case, the experimental evidence supported that the S_1 of APO leads to O–O splitting and higher excited states lead to singlet molecular oxygen [22]. In the present system, transitions higher in energy are also clearly characterized by $\pi_{cc}\pi^*_{cc}$ excitations and according to Kearns correlation diagrams should be responsible for singlet oxygen generation. Excitation to the lowest excited state should cleavage the endoperoxide bridge but it cannot be disregarded that singlet oxygen is also produced.

3.3 Photochemistry

Regardless of the localization of the $\pi^*_{oo}\sigma^*_{oo}$ state, both APO [25] and CHDEPO [26] present a 4CI where additionally four triplet states are also strictly degenerate. This high-order degeneracy point is reached in the process of homolytic O–O dissociation, independently whether it is directly accessed from the S_1 (as in APO [27]) or indirectly accessed from higher excited states. In the present section, we discuss the possibility of this degeneracy point in **1**, associated with the 1A″ state.

Since degeneracy points can only be obtained using multiconfigurational methods, we restrict our analysis to the use of CASSCF. In this case, the 1A″ state is predominantly a $\pi^*_{oo}\sigma^*_{oo}$ state. For this reason and computational sake, the lowest excited state of **1** is described with a minimal active space that includes only the peroxide orbitals (σ_{oo}, π_{oo}, π^*_{oo}, and σ^*_{oo}), as done in Refs. [19, 25, 27]. This CASSCF(6,4) calculation is used to perform a MEP from the S_1 state. This calculation leads directly to a two-state degeneracy point or CI between the S_1 and S_0. The geometry of this CI is shown in Fig. 4. The O–O

distance increases from 1.47 Å in the ground state equilibrium structure to 2.41 Å in the CI. The homolysis of the peroxide group in **1** is obviously hindered by the *o*-fluorine-phenyl moiety so that the O · · · O bond is less stretched than in APO [25] (3.57 Å) or in CHDEPO [26] (4.85 Å). This nuclear interaction induces a slight movement of the *ortho*-fluorine-phenyl substituent out of the xz-plane. The opening of the peroxide bridge is accompanied by a disrotation of the CRO· groups (R=H, *o*-fluorine-phenyl) in different extents (22.4° of CHO· versus 4.9° of the CCO·), and a contraction of 0.81 Å and 0.62 Å in the C-O bonds. Due to additional steric hindrances, similar structures should be expected for endoperoxides **2** and MDHPO (recall Fig. 1).

Cleavage of the peroxide bridge leads to a biradical species. Accordingly, the molecular orbitals (σ_{oo}, π_{oo}, π^*_{oo} and σ^*_{oo}) should convert into the atomic *p* orbitals (p_y, p_y', p_z, and p_z') [25]. However, as seen in Fig. 5, due to the substitution in 9-position and the impossibility of freely stretching the O–O bond, the σ_{oo} and π_{oo} orbitals retain some molecular character at the geometry of the CI. As in APO [25] and CHDEPO [26], this geometry is not only a CI between S_0 and S_1, but a point where the first four singlet states (S_0, S_1, S_2, and S_3) and the four triplet states (T_1, T_2, T_3, and T_4) come very close. Note that the S_n (and the corresponding T_n) labeling should *not* be correlated with the order of the states at the Franck–Condon geometry reported in Sect. 3.2; here, the states are those obtained in the subspace of the (6,4) active space for this particular structure. In Table 5, the relative energies and electronic configuration of each state at MS-CASPT2/SA4-CASSCF(6,4) level of theory are reported. The obtained singlet and triplet states are mixtures of several configurations. Due to the hindered opening of the O–O bond and the fact that the atomic orbitals are not completely formed, in this case, the states are not exactly degenerate. Although the S_2 and S_3 are close to each other in energy, they are 0.35 eV and 0.39 eV, respectively, above the ground state. Interestingly, at this geometry, the lowest triplet state T_1 is below the S_0 at CASSCF level of theory, so that the ground state of this structure is a triplet state. Upon inclusion of dynamical correlation, both S_0 and T_1 states are strictly degenerate. At this level of theory, the higher excited triplet states T_2, T_3, and T_4 are degenerate within 0.05 eV.

Finally, we computed SOCs among the eight states. Since in this case the energy gaps between the states are not affected by adding dynamical correlation, the SOCs are generated at the CASSCF level of theory. As seen in Table 5 the S_0 couples with the T_1 and T_3, the S_1 with the T_2, the S_2 with the T_3, and the S_3 with T_2. All calculated SOCs are in the range between 38 cm^{-1} and 73 cm^{-1}. Even if these numbers are only computed at CASSCF level of theory, they indicate that ISC should play a role in the photochemistry of this endoperoxide.

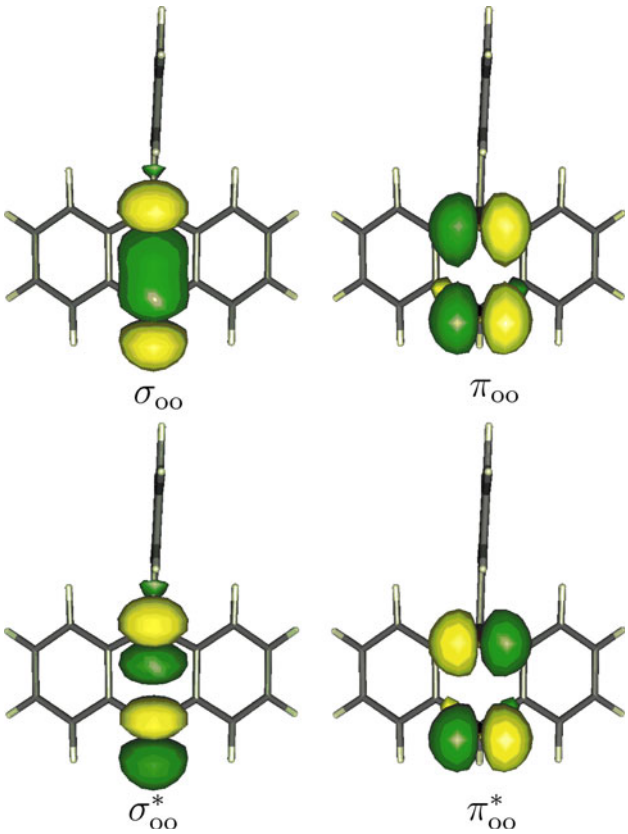

Fig. 5 Optimized orbitals at the conical intersection calculated at SA(6)-CASSCF (6, 4)/ANO-S level of theory

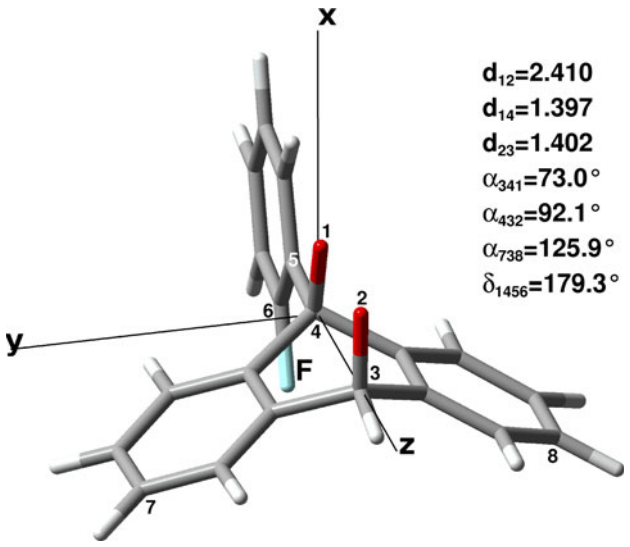

Fig. 4 Conical intersection between S_0 and S_1 calculated with a MEP calculation at CASSCF (6, 4)/ANO-S level of theory. Bond lengths in Ångströms and bond and dihedral angles in degrees

Table 5 Excitation energies ΔE (in eV) at the SA(4)-CASSCF(6,4) and MS-CASPT2 levels of theory computed at the geometry of the S_1/S_0 conical intersection, main contributions to CASSCF wave functions, and the spin-orbit couplings between the singlet and triplet states of 1

State	E/eV		Configuration	c^2/%	Coupled state	E_{SOC}/cm^{-1}
	CASSCF	MS-CASPT2				
S_0	0.00	0.00	$\sigma_{oo}^{2}\ \pi_{oo}^{2}\ \pi_{oo}^{*\,2}\ \sigma_{oo}^{*\,0}$	64	T_1	38
			$\sigma_{oo}^{0}\ \pi_{oo}^{2}\ \pi_{oo}^{*\,2}\ \sigma_{oo}^{*\,2}$	35	T_3	60
T_1	−0.02	0.00	$\sigma_{oo}^{2}\ \pi_{oo}^{2}\ \pi_{oo}^{*\,1}\ \sigma_{oo}^{*\,1}$	44		
			$\sigma_{oo}^{2}\ \pi_{oo}^{1}\ \pi_{oo}^{*\,2}\ \sigma_{oo}^{*\,1}$	18		
			$\sigma_{oo}^{1}\ \pi_{oo}^{2}\ \pi_{oo}^{*\,1}\ \sigma_{oo}^{*\,2}$	14		
			$\sigma_{oo}^{1}\ \pi_{oo}^{1}\ \pi_{oo}^{*\,2}\ \sigma_{oo}^{*\,2}$	27		
S_1	0.03	0.05	$\sigma_{oo}^{2}\ \pi_{oo}^{2}\ \pi_{oo}^{*\,1}\ \sigma_{oo}^{*\,1}$	33	T_2	64
			$\sigma_{oo}^{1}\ \pi_{oo}^{2}\ \pi_{oo}^{*\,2}\ \sigma_{oo}^{*\,1}$	25		
			$\sigma_{oo}^{1}\ \pi_{oo}^{2}\ \pi_{oo}^{*\,1}\ \sigma_{oo}^{*\,2}$	20		
			$\sigma_{oo}^{1}\ \pi_{oo}^{1}\ \pi_{oo}^{*\,2}\ \sigma_{oo}^{*\,2}$	22		
T_2	0.24	0.34	$\sigma_{oo}^{2}\ \pi_{oo}^{1}\ \pi_{oo}^{*\,1}\ \sigma_{oo}^{*\,2}$	8		
			$\sigma_{oo}^{1}\ \pi_{oo}^{2}\ \pi_{oo}^{*\,2}\ \sigma_{oo}^{*\,1}$	91		
S_2	0.30	0.35	$\sigma_{oo}^{2}\ \pi_{oo}^{2}\ \pi_{oo}^{*\,0}\ \sigma_{oo}^{*\,2}$	53	T_3	48
			$\sigma_{oo}^{2}\ \pi_{oo}^{1}\ \pi_{oo}^{*\,2}\ \sigma_{oo}^{*\,1}$	47		
T_3	0.30	0.37	$\sigma_{oo}^{2}\ \pi_{oo}^{2}\ \pi_{oo}^{*\,1}\ \sigma_{oo}^{*\,1}$	19		
			$\sigma_{oo}^{2}\ \pi_{oo}^{1}\ \pi_{oo}^{*\,2}\ \sigma_{oo}^{*\,1}$	39		
			$\sigma_{oo}^{1}\ \pi_{oo}^{2}\ \pi_{oo}^{*\,2}\ \sigma_{oo}^{*\,1}$	29		
			$\sigma_{oo}^{1}\ \pi_{oo}^{1}\ \pi_{oo}^{*\,2}\ \sigma_{oo}^{*\,2}$	12		
S_3	0.32	0.39	$\sigma_{oo}^{2}\ \pi_{oo}^{2}\ \pi_{oo}^{*\,1}\ \sigma_{oo}^{*\,1}$	27	T_2	52
			$\sigma_{oo}^{2}\ \pi_{oo}^{1}\ \pi_{oo}^{*\,2}\ \sigma_{oo}^{*\,1}$	31		
			$\sigma_{oo}^{1}\ \pi_{oo}^{2}\ \pi_{oo}^{*\,1}\ \sigma_{oo}^{*\,2}$	24		
			$\sigma_{oo}^{1}\ \pi_{oo}^{1}\ \pi_{oo}^{*\,2}\ \sigma_{oo}^{*\,2}$	18		
T_4	0.31	0.39	$\sigma_{oo}^{2}\ \pi_{oo}^{1}\ \pi_{oo}^{*\,1}\ \sigma_{oo}^{*\,2}$	91	T_1	73
			$\sigma_{oo}^{1}\ \pi_{oo}^{2}\ \pi_{oo}^{*\,2}\ \sigma_{oo}^{*\,1}$	9	T_3	44

4 Conclusions

In this paper, we have investigated the vertical excited states of a substituted anthracene endoperoxide (*o*-fluorine-phenyl-9-anthracene-9,10-endoperoxide, **1**) and its 9,10-bisarylanthracene analog **2** (see Fig. 1), which is a substrate for a molecular switch flipped by oxygen [29]. Significant effort was put on identifying the position of the states associated with the homolysis of the endoperoxide group with respect to the states which generate molecular singlet oxygen. To this aim, the electronic excited states of **1** were calculated with multiconfigurational methods and compared with the results of CC2 and TD-DFT approaches. Among the functionals tested, it is shown that the best performance is obtained when using B3LYP(32), a functional with 32 % amount of exact exchange. Due to the large size of **2**, its vertical excited states are only computed with B3LYP(32).

The multiconfigurational calculations in **1** are done with the RASPT2/RASSCF prescription and compared with CASPT2/CASSCF, where two different active spaces designed to capture different parts of the spectrum need to be employed: either the local excitations within the peroxide group, the anthracene body and CT between them are obtained, or excitations within the whole aromatic π-system, including the phenyl group, but excluding the orbitals in the peroxide moiety are calculated. The advantage of RASSCF is that it allows employing a larger active space, including all the endoperoxide orbitals and most of the π-system of the anthracene and phenyl group simultaneously.

The RASPT2 calculations show that the lowest excited state of **1** at 4.44 eV is mostly of $\pi_{oo}^{*}\sigma_{oo}^{*}$ nature and thus should correspond to direct O–O homolytic dissociation and associated rearrangement products. Higher excited states are related to excitations into the aromatic π-system coming from either the anthracene fragment or the *o*-fluorine-phenyl moiety. Such states are associated with the production of singlet oxygen, although competing non-radiative pathways could also deliver rearrangement products [25]. The two CASPT2/CASSCF calculations carried out with different active spaces complement to each other and in general, the energies and assignment of the obtained excited states are in agreement with those obtained with RASPT2. However, some states are missing as a consequence of the chosen (or not chosen) orbitals.

The excited states obtained by CC2 are in accordance with the RASPT2 results. The main difference concerns the lowest 1A″ (S_1) state because the fraction of the $\pi_{oo}^{*}\pi_{an}^{*}$

versus $\pi^*_{oo}\sigma^*_{oo}$ excitation is considerably enhanced. The order of the remaining $\pi^*_{oo}\pi^*_{an}$, $\pi_{an}\pi^*_{an}$ and $\pi_{ph}\pi^*_{ph}$ states is akin to the order of states predicted by the multiconfigurational methods. The excited states higher in energy were CT states of either $\pi^*_{oo}\pi^*_{an}$ or $\pi^*_{oo}\pi^*_{ph}$ character.

The TD-DFT calculations were carried out with BP86, CAM-B3LYP, and B3LYP(32). The pure functional BP86 considerably underestimates CT states of $\pi^*_{oo}\pi^*_{an}$ and $\pi^*_{oo}\pi^*_{ph}$ character and thus seven states are wrongly predicted below the $\pi^*_{oo}\sigma^*_{oo}$ state, which should be the S_1 according to any of the multiconfigurational and CC2 calculations performed. CAM-B3LYP and B3LYP(32) give reasonable results in comparison with the multiconfigurational methods. The position of the S_1 state is predicted correctly but with an intermediate mixture of $\pi^*_{oo}\sigma^*_{oo}$ and $\pi^*_{oo}\pi^*_{an}$ excitations. The order of the following $\pi\pi^*$ states resembles the CASPT2 and RASPT2 data. Both CAM-B3LYP and B3LYP(32) predict the CT states ($\pi^*_{oo}\ \pi^*_{an}$ and $\pi^*_{oo}\pi^*_{ph}$) at higher energies, being those of B3LYP(32) in closer agreement with the multiconfigurational ones.

In summary, we have found that RASPT2, even if is not free from limitations, is able to model simultaneously excitations of very different character (local and CT) and therefore can be a powerful method to compute excited states in large molecules which require large active spaces. In view of the three different partitions and the added flexibility in comparison with CASPT2, it is often difficult to find general purpose strategies to compute excited states. Accurate results can only be obtained as long as a wise selection of the active orbitals is made in the corresponding RAS1, RAS2, and RAS3 configurational space. In the case of the present molecule, this requires that the RAS2 is not empty but contains the orbitals where the most important transitions take place. The CC2 results corroborate the RASPT2 ones, while the use of TD-DFT in endoperoxides is only recommended in conjunction with functionals that contain an intermediate amount of exact exchange, such as CAM-B3LYP or B3LYP(32), a functional with 32 % of exact exchange.

Because B3LYP(32) seems to be a reasonable good alternative to expensive CC2 or RASPT2 calculations, this method has been employed in the larger compound **2**. Essentially, both endoperoxides show the same spectrum, with a very small blueshift in the energies of the lowest excited states of **2**. Therefore, a very similar photochemical behavior is expected in both molecules. According to the different calculations used in **1**, it seems reasonable to assume that singlet oxygen is generated when exciting states higher than S_1 while S_1 should be responsible for homolytic dissociation of the endoperoxide bridge; however, singlet oxygen from the S_1 state cannot be completely neglected. To investigate further the splitting of O–O bond, a MEP computation from the $1A''$ (S_1) Franck–Condon geometry has been done in **1**, finding a CI between the S_1 and the electronic ground state S_0. This point is close to a degeneracy point between four singlets and four triplets, as predicted in other endoperoxides [25, 26]. However, in the present molecule, the degeneracy among the eight states is not perfect due to the sterical hindrance of the *o*-fluorine-phenyl group with the peroxide group and such a hindrance should also exist in **2** or in MDHPO, indicating that O–O splitting is not as efficient as, e.g., in APO. Substantial spin-orbit couplings among the singlet and triplet states point to possible intersystem crossing and relaxation via triplet states. Since the competing O–O homolysis is partially quenched by the presence of the bulky substituent, it might be argued that such compounds could be more efficiently employed in photodynamic therapy to produce singlet oxygen. However, more detailed calculations on the deactivation paths using dynamical methods should be employ to ratify such a behavior. Only combining quantum chemistry and reaction dynamics, it is possible to quantify quantum yields of the competing pathways and to predict which paths are really chosen by the system under light irradiation.

Acknowledgments This work is supported by the Deutsche Forschungsgemeinschaft (GO 1059/6-1). All the calculations have been performed at the Universitätsrechenzentrum of the Friedrich-Schiller University of Jena and at the HP computers of the Theoretical Chemistry group at the University of Vienna.

References

1. DeRosa MC, Crutchley RJ (2002) Coord Chem Rev 233/234:351–357
2. Aubry JM, Pierlot C, Rigaudy J, Schmidt R (2003) Acc Chem Res 36:668–675
3. Choea E, Min DB (2006) Crit Rev Food Sci Nutr 46:1–22
4. Henderson BW, Dougherty T (1992) Photochem Photobiol 55:145–157
5. Foote CS (1984) Mechanisms of photooxidation. In: Doiron DG, Gomer CJ (eds) Porphyrin localization and treatment of tumors. Alan R. Liss, Inc, pp 3–18
6. Schmidt R, Schaffner K, Trost W, Brauer HD (1984) J Am Chem Soc 88:956–958
7. Blumenstock T, Comes FJ, Schmidt R, Brauer HD (1986) Chem Phy Lett 127:452–455
8. Jesse J, Comes FJ, Schmidt R, Brauer HD (1989) Chem Phy Lett 160:8–12
9. Jesse J, Markert R, Comes FJ, Schmidt R, Brauer HD (1990) Chem Phy Lett 166:95–100
10. Brauer HD, Schmidt R (2000) J Phys Chem A 104:164–165
11. Schmidt R (2012) Photochem Photobiol 11:1004–1009
12. Eisenthal KB, Turro NJ, Dupuy CG, Hrovat DA, Langan J, Jenny TA, Sitzmann EV (1986) J Phys Chem 90:5168–5173
13. Klein A, Gudipati MS (1999) J Phys Chem A 103:3843–3853
14. Corral I, González L, Lauer A, Freyer W, Fidder H, Heyne K (2008) Chem Phys Lett 452:67–71
15. Gudipati MS, Klein A (2000) J Phys Chem A 104:166–167

16. Kearns RD (1969) J Am Chem Soc 91:6554–6563
17. Kearns RD, Khan AU (1969) Photochem Photobiol 10:193–210 / Khan69
18. Corral I, González L (2008) J Comput Chem 29:1982–1991
19. Corral I, González L (2007) Chem Phys Lett 446:262–267
20. Martínez-Fernández L, González L, Corral I (2011) Comput Theoret Chem 975:13–19
21. Donkers RL, Workentin MS (2004) J Am Chem Soc 126:1688–1698
22. Fidder H, Lauer A, Freyer W, Koeppe B, Heyne K (2009) J Phys Chem A 104:6289–6296
23. Rigaudy J, Breliere C, Scribe P (1978) Tetrahedron Lett 7:687–690
24. Ernsting NP, Schmidt R, Brauer H (1990) J Phys Chem 94:5252–5255
25. Mollenhauer D, Corral I, González L (2010) J Phys Chem Lett 1:1036–1040
26. Corral I, González L (2010) Chem Phys Lett 499:21–25
27. Assmann M, Worth GA, González L (2012) J Chem Phys 137:22A524-1–22A524-12
28. Lauer A, Dobryakov AL, Kovalenko SA, Fidder H, Heyne K (2011) . Phys Chem Chem Phys 13:8723–8732
29. Zehm D, Fudicker W, Linker T (2007) Angew Chem Int Ed 46:7689–7692
30. González L, Escudero D, Serrano-Andrés L (2012) Chem Phys Chem 13:28–51
31. Dreuw A, Head-Gordon M (2004) J Am Chem Soc 126:4007–4016
32. Becke AD (1988) Phys Rev A 38:3098–3100
33. Lee C, Yang W, Parr RG (1988) Phys Rev B 37:785–789
34. Christiansen O, Koch H, Jørgensen P (1995) Chem Phys Lett 243:409–418
35. Malmqvist PÅ, Rendell A, Roos BO (1990) J Phys Chem 94:5477–5482
36. Olsen J, Roos BO, Jørgensen P, Jensen HJA (1988) J Chem Phys 89:2185–2192
37. Malmqvist PÅ, Pierloot K, Shahi ARM, Cramer CJ, Gagliardi L (2008) J Chem Phys 128:204109-1–204109-10
38. Manni GL, Aquilante F, Gagliardi L (2011) J Chem Phys 134:034114–034118
39. Sauri V, Serrano-Andrs L, Shahi ARM, Gagliardi L, Vancoillie S, Pierloot K (2011) J Chem Theory Comput 7:153–168
40. Escudero D, González L (2012) J Chem Theory Comput 8:203–213
41. Becke AD (1993) J Chem Phys 98:5648–5652
42. Hariharan PC, Pople JA (1973) Theor Chim Acta 28:213–222
43. Frisch MJ, Trucks GW, Schlegel HB, Scuseria GE, Robb MA, Cheeseman JR, Scalmani G, Barone V, Mennucci B, Petersson GA, Nakatsuji H, Caricato M, Li X, Hratchian HP, Izmaylov AF, J Bloino GZ, Sonnenberg JL, Hada M, Ehara M, Toyota K, Fukuda R, Hasegawa J, Ishida M, Nakajima T, Honda Y, Kitao O, Nakai H, Vreven T, Montgomery JJA, Peralta JE, Ogliaro F, Bearpark M, Heyd JJ, Brothers E, Kudin KN, Staroverov VN, Kobayashi R, Normand J, Raghavachari K, Rendell A, Burant JC, Iyengar SS, Tomasi J, CossiM, Rega N,MillamJM, KleneM, Knox JE, Cross JB, Bakken V, Adamo C, Jaramillo J, Gomperts R, Stratmann RE, O Yazyev AJA, R Cammi CP, Ochterski JW, Martin RL, Morokuma K, Zakrzewski VG, Voth GA, Salvador P, Dannenberg JJ, Dapprich S, Daniels AD, Farkas O, Foresman JB, Ortiz JV, Cioslowski J, Fox DJ (2009) *Gaussian 09*, Revision A.1, Gaussian, Inc., Wallingford, CT
44. Yanai T, Tew DP, Handy NC (2004) Chem Phys Lett 393:51–57
45. Perdew JP (1986) Phys Rev B 33:8822–8824
46. Feyereisen M, Fitzgerald G, Komornicki A (1993) Chem Phys Lett 208:359–363
47. T H Dunning J (1971) J Chem Phys 55:716–723
48. Ahlrichs R, Bar M, Haser M, Horn H, Kolmel C (1989) Chem Phys Lett 162:165–169
49. Roos BO (1987) In Ab initio methods in quantum chemistry II. Wiley-VCH, Chinester
50. Finley J, Malmqvist PÅ, Roos BO, Serrano-Andrés L (1998) Chem Phys Lett 288:299–306
51. Aquilante F, Vico LD, Ferré N, Ghigo G, Malmqvist P, Neogrády P, Pedersen TB, Pitonak M, Reiher M, Roos BO, Serrano-Andrés L, Urban M, Veryazov V, Lindh R (2010) J Comput Chem 31:224–247
52. Veryazov V, Widmark PO, Serrano-Andrés L, Lindh R, Roos BO (2004). Int J Quantum Chem 100:626–635
53. Karlström G, Lindh R, Malmqvist PÅ, Roos BO (2003) . Comput Mater Sci 28:222–239
54. Andersson K, Aquilante F, Bernhardsson A, Blomberg MRA, Cooper DL, Cossi M, Devarajan A, L De Vico NF, Fülscher MP, Gaenko A, Gagliardi L, Ghigo G, de Graaf C, Hess BA, Hagberg D, Holt A, Karlström G, Krogh JW, Lindh R, Malmqvist PÅ, Neogrády P, Olsen J, Pedersen TB, Pitonak M, Raab J, Reiher M, Roos BO, Ryde U, Schapiro I, Schimmelpfennig B, Seijo L, Serrano-Andrés L, Siegbahn PEM, Stålring J, Thorsteinsson T, Vancoillie S, Veryazov V, Widmark PO, Wolf A (2011) *MOLCAS*, Release 7.6, Department of Theoretical Chemistry, Lund University
55. Pierloot K, Dumez B, Widmark PO, Roos BO (1995) Theor Chim Acta 90:87–114
56. Aquilante F, Malmqvist P, Pedersen TB, Ghosh A, Roos BO (2008). J Chem Theory Comput 4:694–702
57. Anderson K, Roos BO (1995) Chem Phys Lett 245:215–223
58. Malmqvist P, Roos BO (1989) Chem Phys Lett 155:189–194
59. Malmqvist P, Roos BO, Schimmelpfennig B (2002) Chem Phys Lett 357:230–240